



**HAL**  
open science

## Theoretical model and experimental investigation of current density boundary condition for welding arc study

A. Boutaghane, K. BouhadeF, Flavien Valensi, S. Pellerin, Y. Benkedda

► **To cite this version:**

A. Boutaghane, K. BouhadeF, Flavien Valensi, S. Pellerin, Y. Benkedda. Theoretical model and experimental investigation of current density boundary condition for welding arc study. European Physical Journal: Applied Physics, 2011, 54 (1), 10.1051/epjap/2011100146 . hal-00687330

**HAL Id: hal-00687330**

**<https://hal.science/hal-00687330>**

Submitted on 13 Apr 2012

**HAL** is a multi-disciplinary open access archive for the deposit and dissemination of scientific research documents, whether they are published or not. The documents may come from teaching and research institutions in France or abroad, or from public or private research centers.

L'archive ouverte pluridisciplinaire **HAL**, est destinée au dépôt et à la diffusion de documents scientifiques de niveau recherche, publiés ou non, émanant des établissements d'enseignement et de recherche français ou étrangers, des laboratoires publics ou privés.

# Theoretical model and experimental investigation of current density boundary condition for welding arc study

A Boutaghane<sup>1,3</sup>, K Bouhade<sup>2</sup>, F Valensi<sup>3,4</sup>, S Pellerin<sup>3</sup> and Y Benkedda<sup>1</sup>

<sup>1</sup> Centre de recherche scientifique et technique en soudage et contrôle, CSC, Alger, Algérie

<sup>2</sup> Université des sciences et de la technologie, Houari Boumediene, USTHB, Alger, Algérie

<sup>3</sup> GREMI-Site de Bourges, Université d'Orléans/CNRS, BP 4043, 18028 Bourges cedex 2 - France

<sup>4</sup> LAPLACE-AEPPT, Université Paul Sabatier/CNRS, 31062 Toulouse cedex 9 - France

Correspondent's email address: [stephane.pellerin@univ-orleans.fr](mailto:stephane.pellerin@univ-orleans.fr)

Correspondent's fax number: (33) [0]2 48 70 75 41

**Abstract.** This paper presents results of theoretical and experimental investigation of the welding arc in Gas Tungsten Arc welding (GTAW) and Gas Metal Arc Welding (GMAW) processes. A theoretical model consisting in simultaneous resolution of the set of conservation equations for mass, momentum, energy and current, Ohm's law and Maxwell equation is used to predict temperatures and current density distribution in argon welding arcs. A current density profile had to be assumed over the surface of the cathode as a boundary condition in order to make the theoretical calculations possible. In stationary GTAW process, this assumption leads to fair agreement with experimental results reported in literature with maximum arc temperatures of ~ 21000 K. In contrast to the GTAW process, in GMAW process, the electrode is consumable and non-thermionic, and a realistic boundary condition of the current density is lacking. For establishing this crucial boundary condition which is the current density in the anode melting electrode, an original method is setup to enable the current density to be determined experimentally. High-speed camera (3000 images/sec) is used to get geometrical dimensions of the welding wire used as anode. The total area of the melting anode covered by the arc plasma being determined, the current density at the anode surface can be calculated. For a 330 A arc, the current density at the melting anode surface is found to be of  $5 \times 10^7$  A.m<sup>-2</sup> for a 1.2 mm diameter welding electrode.

**Keywords:** thermal plasma, magnetohydrodynamic, argon arc, GTAW, GMAW process

**PAC's number:** 52.50.-b, 52.65.Kj, 52.70.Kz, 52.75.Hn, 52.77.Fv

*Submitted to: European Physical Journal - Applied Physics*

## 1. Introduction

In arc welding, an electric arc is burning between a “workpiece” and an auxiliary electrode:

- For gas metal arc welding (GMAW) process the auxiliary electrode is welding wire, which is usually the anode (reverse polarity). Heat transfer from the arc and Ohm's heating in the wire melt its tip forming droplets, transferred through the arc to the workpiece used as a cathode.
- For gas tungsten arc welding (GTAW) process, the workpiece, which is usually the anode (straight polarity), locally melts due to heat transfer from the arc, forming a weld pool.

Thermal behaviour of welding arcs and their electrodes can have significant effects on the subsequent weld quality and production rate. Hence, it is desirable to have a theoretical method which can predict the properties of both electrodes and arc plasma as functions of the arc operating conditions.

The behaviour of an arc is governed by a coupled set of physical laws, i.e., Ohm's Law, Maxwell's equations and conservation equations of mass, momentum, energy and electrical charge [1, 2]. The modelling of arc welding processes has been reported by a number of researchers [2-16]. Most early numerical models have treated either only the arc plasma [2-7] or only the weld pool [8-14]. For the arc plasma, a plane surface of the solid anode has been set to be a bottom boundary for the electric potential and temperature which are given as the boundary conditions. The tungsten cathode has been assumed to be at a uniform temperature as a boundary condition and the current density distribution on the cathode has been also given as another boundary condition to the calculations of the arc plasma. For calculations of the weld pool, the distributions of heat flux and current density to be specified at the anode surface have been required. More recent models have combined the arc plasma and the weld pool for stationary welding [15, 16], but the calculations of the arc plasma and the weld pool were made separately, without interaction between the plasma and the weld pool. The first completely unified models of the gas tungsten arc were for arcs with solid anodes made of copper cooled by water [17, 18]. The unified models give temperatures and current densities in the whole region of the arc, i.e. for the tungsten cathode, the arc plasma and the anode. These basic models and procedures were extended to include melting of the anode, with inclusion of convective effects in the molten anode, for predicting the GTAW properties [18]. A unified electrode-arc weld-pool treatment, including effects of depression of the weld-pool surface due to the arc pressure, has been presented by Haidar [19]. Generally, it is assumed that the arc plasma at atmospheric pressure is a fluid [2-7, 15-17]. The magnetohydrodynamic (MHD) approximation, which includes force terms due to the magnetic field in the momentum equations, solves for pressure, temperature, velocity and electric potential through the four conservation equations of mass, momentum, energy and current. If we assume rotational symmetry around the arc axis, the system can be represented by cylindrical coordinates.

Compared with the GTAW arc plasma, modelling of the GMAW has been far less addressed. Relatively few researchers have attempted to combine the various aspects of the physical modelling in order to determine the overall behaviour of the GMAW process. In these previous papers, the anode melting rate has not been considered and droplets have been simply represented either by truncated ellipsoids or by truncated spheres. This is only an indication of trends rather than the actual behaviour of droplets formation, since a number of severe simplifications and assumptions have been introduced [24, 31]. Hence it is desirable to develop a GMAW model that takes the properties of the welding arc, the melting anode as well as the droplet formation into consideration.

In the first part of this paper, solutions of the conservation equations in the magnetohydrodynamic (MHD) approximation are presented in stationary state for GTAW process with argon shielding gas at atmospheric pressure. Detailed calculations are presented for 100 A, 200 A and 300 A arcs in argon at atmospheric pressure. In the second part of this paper, particular attention to the molten welding wire of Gas Metal Arc Welding (GMAW) process is made for further GMAW model. The GTAW arc model is adapted to represent the GMAW arc, taking into account the change of polarity, to calculate the arc column temperatures by assuming a realistic current density distribution on the anode spot which is determined experimentally. An original method is proposed in this second part of this paper

to determine the shape and the dimensions of the molten anode by using high-speed camera (3000 images/sec). Geometrical dimensions of a 1.2 mm molten welding wire are markedly presented for a 330 A arc. It is worth mentioning that current density in GMAW higher than  $10^7 \text{ A.m}^{-2}$  seems to be not justified for welding current less than 330 A. To the best of our knowledge, it is for the first time the molten electrode dimensions are thoroughly presented. The boundaries of the wire anode region change with time, depending upon the shape of the droplet and the melting rate of the anode. Contour detection of arc images, obtained by high-speed video camera, is performed to represent these geometrical boundary conditions which are of key importance for further semi-empirical GMAW model.

## 2. Theory

Figure 1 shows the computational domain used in the GTAW process. The presence of an electric field between the cathode (a tungsten rod) and the anode (metal workpiece) causes the passage of an electric current through the ionized plasma region. The interaction of the arc current with its own magnetic field leads, in arc regimes of variable cross section, to the phenomena of induced plasma jets. The cathode region of a free-burning arc, for example, acts as an electromagnetic pump drawing gas from the surroundings and ejecting it toward the anode in the form of a jet. Due to the electrical resistance of the plasma, the energy produced by the current keeps the plasma in the ionized state and provides the heating mechanism for the welding process. For modelling this complex welding arc, some assumptions must be made:

1. The arc is axially symmetric so that the equations can be written in two-dimensional cylindrical coordinates.
2. The plasma is in local thermodynamic equilibrium (LTE).
3. The arc is in the steady state and the flow is laminar.
4. The plasma is optically thin.

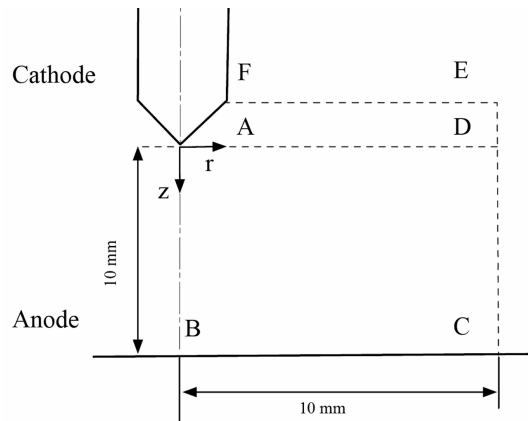


**Figure 1.** Arc-electrode domain.

### 2.1. Governing equations

Based on these assumptions, the conservation equations governing the arc region may be expressed in cylindrical coordinates as follow [2, 24]:

- Current continuity equation in terms of electric potential:

$$\nabla^2 V = \frac{\partial}{\partial z} \left( \sigma \frac{\partial V}{\partial z} \right) + \frac{1}{r} \frac{\partial}{\partial r} \left( \sigma r \frac{\partial V}{\partial r} \right) = 0 \quad (1)$$

where  $\sigma$  is the electrical conductivity; and  $V$  the electrical potential.

- The current density is given by:

$$J_r = -\sigma \frac{\partial V}{\partial r} \quad \text{and} \quad J_z = -\sigma \frac{\partial V}{\partial z} \quad (2)$$

where  $J_r$  and  $J_z$  are the radial current density and the axial current density, respectively.

- Since the current distribution is axisymmetric, the self-induced magnetic field is given by the following relation from Ampere's law:

$$B_\theta = \frac{\mu_0}{r} \int_0^r J_z \xi d\xi \quad (3)$$

where  $\mu_0 = 4 \times 10^{-7} \text{ H.m}^{-1}$  is the permeability of free space.

- The Lorenz force components are given as:

$$F_r = -B_\theta J_z \quad \text{and} \quad F_z = -B_\theta J_r \quad (4)$$

where  $F_r$  is the radial component and  $F_z$  is the axial component

- Mass conservation:

$$\frac{1}{r} \frac{\partial}{\partial r} (r\rho v) + \frac{\partial}{\partial z} (\rho u) = 0 \quad (5)$$

where  $\rho$  is the gas density; and  $u$  and  $v$  are the axial and radial velocities, respectively.

- Radial momentum equation:

$$\begin{aligned} \frac{\partial(\rho u)}{\partial t} + \frac{1}{r} \frac{\partial(r\rho v^2)}{\partial r} + \frac{\partial(\rho uv)}{\partial z} = & -\frac{\partial P}{\partial r} - j_z B_\theta + \frac{1}{r} \frac{\partial}{\partial r} (2r\mu \frac{\partial v}{\partial r}) \\ & + \frac{\partial}{\partial z} (\mu \frac{\partial v}{\partial z} + \mu \frac{\partial u}{\partial r}) - 2\mu \frac{v}{r^2} \end{aligned} \quad (6)$$

and axial momentum equation:

$$\begin{aligned} \frac{\partial(\rho v)}{\partial t} + \frac{1}{r} \frac{\partial(r\rho vu)}{\partial r} + \frac{\partial(\rho u^2)}{\partial z} = & -\frac{\partial P}{\partial z} + j_r B_\theta + \frac{\partial}{\partial z} (2\mu \frac{\partial u}{\partial z}) \\ & + \frac{1}{r} \frac{\partial}{\partial r} (r\mu \frac{\partial v}{\partial z} + r\mu \frac{\partial u}{\partial r}) + \rho g \end{aligned} \quad (7)$$

where  $P$  is the pressure;  $\mu$  is the dynamic viscosity; and  $g$  is the gravitational acceleration.

- Energy equation:

$$\begin{aligned} \rho c_p \left( u \frac{\partial T}{\partial z} + v \frac{\partial T}{\partial r} \right) = & \frac{\partial}{\partial z} \left( k \frac{\partial T}{\partial z} \right) + \frac{1}{r} \frac{\partial}{\partial r} \left( kr \frac{\partial T}{\partial r} \right) + \frac{J_z^2 + J_r^2}{\sigma} \\ & + \frac{5}{2} \frac{k_B}{e} \left( J_z \frac{\partial T}{\partial z} + J_r \frac{\partial T}{\partial r} \right) - S_R \end{aligned} \quad (8)$$

where  $T$  is the temperature;  $S_R$  is the radiation heat loss;  $c_p$  is the specific heat at constant pressure;  $k$  is the thermal conductivity;  $k_B$  is the Boltzmann constant; and  $e$  is the electronic charge.

The energy equation contains, from left to right, two convection terms, two conduction terms, the joule-heating term, an additional term that represents the transport of electron enthalpy

due to the drift of the electrons and the radiation term  $S_R$ .

## 2.2. Boundary conditions

The calculation domains and the boundary conditions used in this analysis are specified with reference to Figure 1 in Table 1. The calculation domain for  $u$ ,  $v$  and  $T$  is chosen as the area ABCD. Therefore, the domain for  $V$  is chosen as the smaller area ABCD, since the exact boundary condition for  $V$  along the line FA is unknown.

**Table 1.** Boundary Conditions

	AB	BC	CE	EF	FA	DA
$V$	$\frac{\partial V}{\partial r} = 0$	$V = C^{te}$	$\frac{\partial V}{\partial r} = 0$			Equation (9)
$u$	$\frac{\partial u}{\partial r} = 0$	$u = 0$	$\frac{\partial u}{\partial r} = 0$	$\frac{\partial \rho u}{\partial r} = 0$	$u = 0$	
$v$	$v = 0$	$v = 0$	$\frac{\partial v}{\partial r} = 0$	$v = 0$	$v = 0$	
$T$	$\frac{\partial T}{\partial r} = 0$	$T_{exp} = 2200$ K [20, 21, 26]	1000 K [22]	1000 K [2, 6, 17]	3000 K [2, 6, 17]	

Due to symmetry, only a half of the flow domain was considered for the calculation. Along the centreline AB, symmetry conditions are used, zero velocities are specified along the solid boundaries BC and FA.

Along the far field boundary CE, zero radial gradients for all variables are specified unless for the temperature, which is set to 1000 K [22]. A constant electrical potential is specified along the anode surface BC because the anode is assumed to be a perfect conductor relative to the plasma. Experimental data of Bloch-Bolten and Eagar [20] and Cieslak *et al.* [21] showed that the maximum surface temperature for steel weld pool is approximately 500 K below the boiling temperature. In this study, therefore, we set a constant temperature of 2200 K at the cathode surface as suggested by Tanaka and Lowke [26].

Along the boundary EF, the temperature is taken as 1000 K [2, 6, 17] and the radial velocity component is neglected. At the cathode surface FA, the temperature is assumed to be 3000 K [2, 6, 5, 17] except at the point where the current emerges from the cathode. The cathode spot itself cannot be easily modelled because of non-LTE effects. The cathode sheath is typically 0.1 mm wide, and in this region, electrons are heated from 3000 K to 21000 K [5, 22, 30]. Since our model describes only the positive column, we do not take into account cathode sheath effects, and thus we assume that the temperature of the cathode spot is 21000 K [2, 5] for all currents. As the cathode spot radius depends on the current, its values are taken from experimental measurements: we set to  $r_h = 0.6$  mm,  $r_h = 0.51$  mm,  $r_h = 0.45$  mm for arc currents of 300 A, 200 A and 100 A respectively [2, 5, 30].

The most critical boundary condition in this modelling is the current density distribution along the line DA. For this region, the current density defines a boundary condition for  $V$ . The profile of the current density is formulated following the representation of Hsu *et al* [2] and Kovitya *et al* [5]. It is assumed to be of the form:

$$J_c = J_0 \exp(-br) \quad (9a)$$

where  $b$  is a constant and the maximum current density is

$$J_0 = \frac{I}{2\pi r_h^2} \quad (9b)$$

The constant  $b$  is determined from:

$$I = 2\pi \int_0^{R_c} J_0 \exp(-br) r dr \quad (10)$$

where  $R_c$  is the cut-off radius of the arc along  $DA$ .  $R_c$  is taken as 3 mm [2] for the evaluation of  $b$ . This choice, however, is not critical because of the assumed exponential decay of the current density in the radial direction.

The material properties of the plasma (density, constant pressure specific heat, viscosity, electrical and thermal conductivities) have been taken from literature [31].

### 3. Numerical method

The method of representing the conservation equations is the finite control volume method formulated for rectangular grid system. The partial differential equations (1) to (8) are solved iteratively by the SIMPLEC numerical procedure as originated by Patankar [1] and used thereafter in several work [2, 27, 31, 35]. To prevent instabilities, we have used upwind method of evaluating the convective terms on the left-hand sides of equations (6)-(8). It is necessary to use relaxation parameter to avoid numerical instabilities. With a relaxation parameter of  $\sim 0.8$ , convergence is generally achieved in  $\sim 300$  iterations.

Actually the electrical potential and the current density calculated by this method, equations (1, 2), have to be adjusted so that the calculated intensity  $I^*$ , equation (12), can be matched with the imposed intensity of the current  $I$ . The intensity of the current  $I^*$ , on one or more sections of the arc, can be calculated by:

$$I^* = \frac{1}{n_p} \sum_{i=1}^{n_p} \iint_{\Sigma_i} \vec{J}^* \cdot d\vec{s} \quad (12)$$

where  $n_p$  is the number of plan and  $\Sigma_i$  is the sectional surface of the plan  $i$ .

We define a constant  $C_V$  which represents the ratio of the imposed current intensity over the calculated current:

$$C_V = \frac{I}{I^*} \quad (13)$$

Then the electrical potential and the current density can be adjusted by:

$$V = C_V V^* \quad \text{and} \quad \vec{J} = C_V \vec{J}^* \quad (14)$$

### 4. Results

Results are presented for 100 A, 200 A and 300 A arcs in argon with a tungsten cathode of 3.2 mm diameter and electrode spacing of  $L = 10$  mm at atmospheric pressure.

In the arc region, the plasma was assumed to be in local thermodynamic equilibrium (LTE), even if departure from LTE can occur in the region immediately surrounding the cathode. Departure from LTE results from a combination of the large temperature gradients and the magnetohydrodynamic properties occurring in the region close to the arc-cathode attachment region. If the electrodes are at temperatures below their melting point, the temperatures of regions adjacent to the electrodes are less than 4000 K and the equilibrium electron density and electrical conductivity are near zero. However, it is believed by many investigators that in practice, non-equilibrium effects such as thermionic emission and ambipolar diffusion can make these regions highly conducting [29, 19, 24]. This region is divided into two subzones [29, 37]: the ionization zone and the space charge zone. The former is used to account for the generation of ions and electrons and extends over a distance of around 0.0075 cm. The latter extends over a distance equivalent to a Debye length,  $\lambda_D = 10^{-6}$  cm, and is used for explaining the sheath formation. Thus, very close to the cathode, the usual continuum approach is no longer valid. In our calculation both the cathode and the anode zone are neglected, this is

supported by the fact that the influence of diffusion processes in the main plasma is small. Besides, a comparison with the experimental results indicates that an optimum mesh size could be used so that, for approximate calculations, non-equilibrium sheaths near the electrodes can be neglected. Lowke *et al.* [27, 29] reported in their modeling of a single temperature argon plasma that neglecting sheath region has little effect on the validity of the results if the mesh size is small enough, and that smaller mesh sizes cause an increase in the error because of significant diffusion effects. In the present calculation, a uniform mesh was used in the whole domain of calculation, this mesh size being 0.05 mm in both the axial and the radial directions. In our case, this value represents the lower cell size to prevent instabilities. However, this mesh size was carefully chosen to represent physical process. Here, we are limited to cases in which convection dominates over diffusion processes, which is usually valid for most parts of the arc.

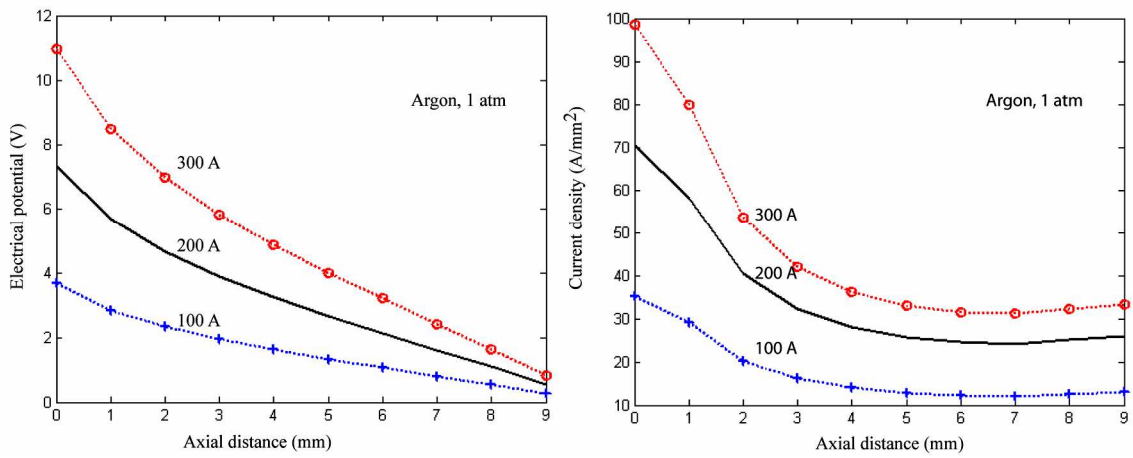


**Figure 2.** Electrical potential and axial current density along the arc axis in a GTAW process.

Figure 2 shows the centreline distribution of the electrical potential and the current density. The calculated total arc voltage is 12.5 V for an arc of 200 A. The corresponding measured value is around 13.1 V [23, 25]. The value calculated by Lowke *et al.* [27] is 12.7 V. The comparison indicates that effects in the cathode sheath of ohmic heating and ionization due to the electric field, which were omitted for the present investigation, were small. The current density is very high near the cathode tip, but decreases rapidly with increasing distance from the cathode. A steep gradient of electrical potential near the cathode tip results in the high current density, which generates a strong magnetic force, and thus, resulting in high arc constriction leading to a strong plasma flow. Thus, the cold neutral atoms injected into the arc due to this effect, caused the cathode zone to be in no LTE state. It has been found that in this cold zone  $n_e/n_e^{LTE}$  is less than 0.5 [19], where  $n_e$  is the electron number density in the cathode region and  $n_e^{LTE}$  is the equilibrium electron number density. Actually, it is well known that the sheath-voltage drop is lower for lower electron number densities in the plasma. In contrast, the high electron number densities at the sheath edge would result in a higher sheath voltage drop [19, 24, 37]. As a result, magnetohydrodynamic models based on LTE assumption may lead to an overestimation of both the temperature and the total voltage drop. In our treatment LTE is assumed throughout the arc plasma, resulting in high electron number densities ( $n_e = n_e^{LTE}$ ) which may lead to overestimation of a sheath voltage. For 200 A arc, the total voltage derived from calculation differs by about 4.5 V, which is almost the sum of the cathode and the anode drop voltage. Hsu *et al.* [37] found the voltage drop in ionization zone of around 4.5 V. Hsu *et al.* [22] found the sum of the cathode and anode fall voltage drop of about 8.7 V. Lowke *et al.* [29] calculated the effect of back diffusion of electrons to the cathode and found that the sheath voltage is increased from 1.5 to 3 V and the total arc voltage is correspondingly increased by 1.5 V. Sansonnens *et al.* [28] estimated that the sum of the cathode and anode voltage is around 2.6 V. Thus, the difference between calculated and measured arc

voltage can be explained by the fact that our calculations do not account for both the cathode and the anode regions.

The calculated isotherms are shown in Figures 3 to 5. The temperature shows a rapid increase in front of the cathode due to ohmic heating, and as the arc spreads (decrease of the current density) the temperature drops to values below 11000 K close to the anode. As expected, the highest temperatures, from 21000 K down to 19000 K, occurred close to the cathode tip for all considered currents as we can see in Figures 3(a) to 5(a). Results are to some extent dependent on the cathode temperature as showed in figures 3(b) to 5(b). Higher cathode temperatures influence the calculations, because the hot cathode tends to broaden the whole arc column and reduces current densities within the arc. At the centre line of the arc and close to the anode and the cathode the arc presents almost the same temperatures for all currents as it can be seen in Figure 6. However, in the column arc the temperatures differ by  $\sim 1000$  K when current changes by 100 A. The arc behaviour is mainly controlled by the welding current: all calculated data, temperatures, voltage drop and axial current density increase when increasing current. The predicted isotherms are in agreement with previous calculations [2, 5, 25]. The discrepancy value at the cathode region is tentatively ascribed to departures from LTE and sheath effects in this zone.

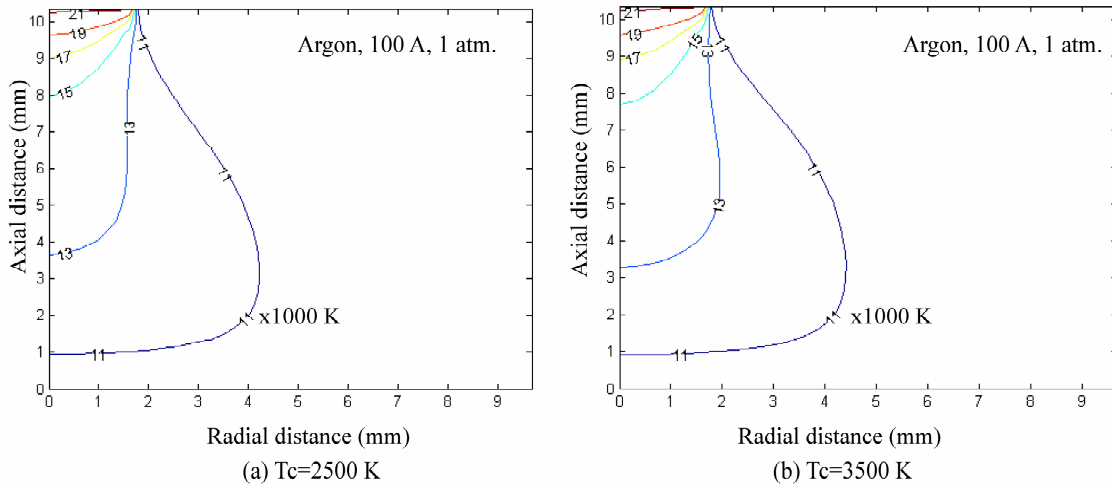


**Figure 3.** Predicted isotherms of a 100 A arc, 10 mm long in argon (GTAW process -  $P = 1$  atm).

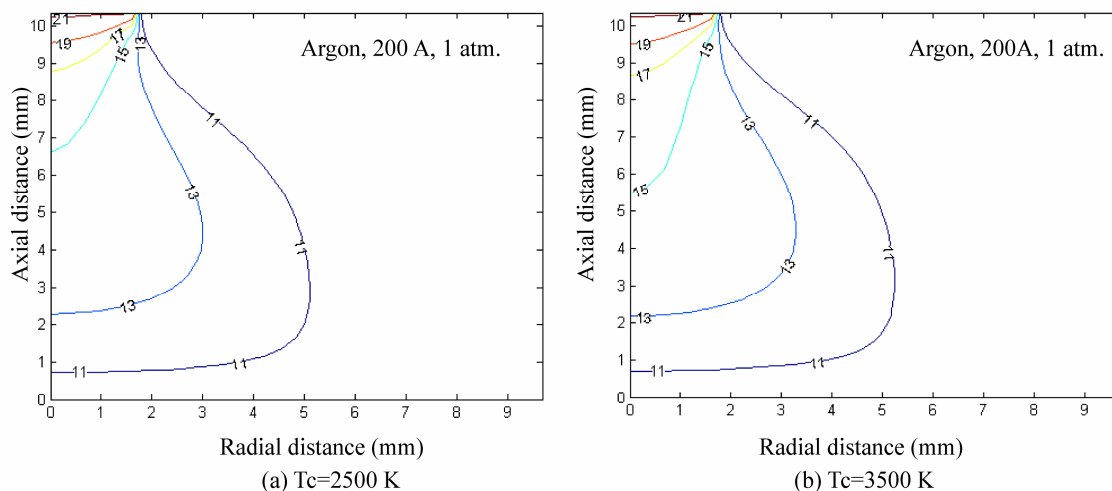


**Figure 4.** Predicted isotherms of a 200 A arc, 10 mm long in argon (GTAW process -  $P = 1$  atm).

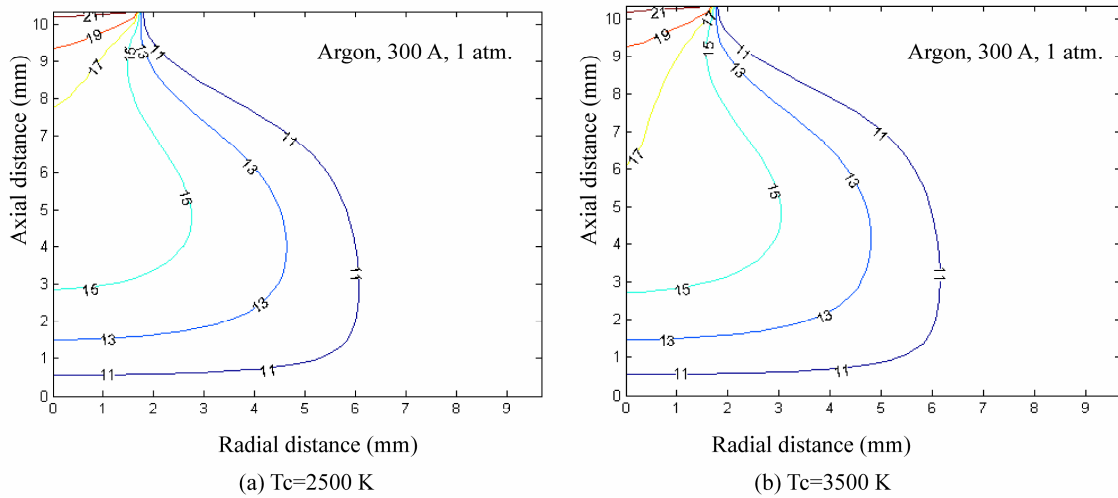


**Figure 5.** Predicted isotherms of a 300 A arc, 10 mm long in argon (GTAW process -  $P = 1$  atm).

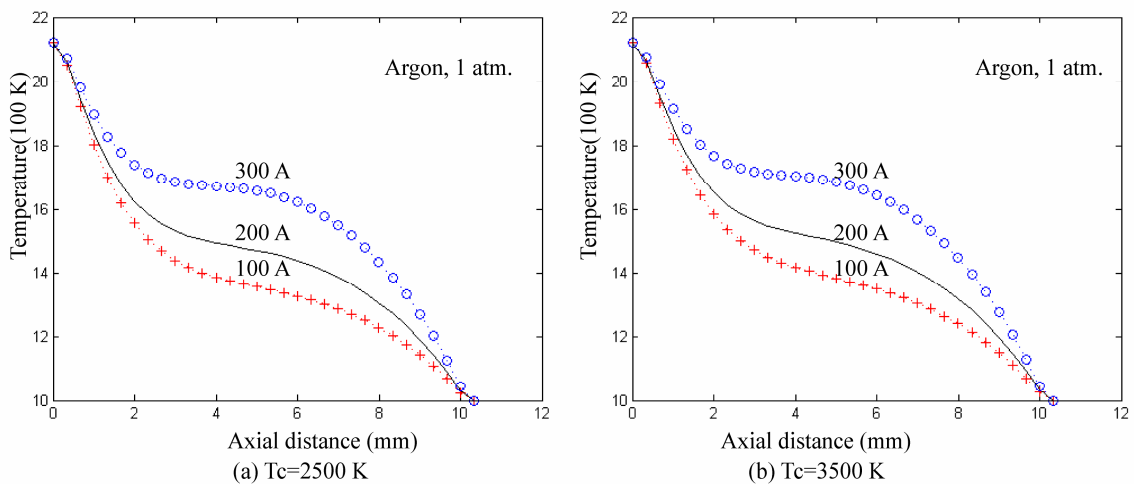


**Figure 6.** Predicted temperatures in arc axis for a 10 mm long arc in argon (GTAW process -  $P = 1$  atm).

It was mentioned above that the thermal behaviour of the GTAW arc is dominated by the current arc, and thus by the current density. Spot radius and hence arc attachment area is of key importance to determine the current density. As showed in section 2, it was necessary to specify the current density profile on the cathode as a boundary condition in order to make the theoretical calculations possible. We showed that the Gaussian distribution of the current density for thermionically emitting cathodes leads to a good prediction of arc properties. In contrast of the GTAW process, the cathode is non-thermionic in GMAW process. The physics of the cathode fall region and the thermal balance at a non-thermionic cathode are not very well understood and thus the current density cannot be easily modeled. In the following sections, experimental model of the anode electrode in GMAW process, electrode positive, is determined for high arc currents, and experimental method of determining current density for a melting electrode is thoroughly presented.

## 5. Experimental electrode model in Gas Metal Arc Welding (GMAW) process

In GMAW process, low-voltage electric arc plasma is maintained between a workpiece and a wire electrode, both of which are melted by the arc. Drops of molten metal detach from the wire electrode in various modes such as globular, repelled globular, projected spray, streaming and rotating transfer.

In contrast with the GTAW process, GMAW process is usually used in reverse polarity i.e. the welding wire electrode is connected to the positive pole (anode). Actually, the arc configuration is more stable in the reverse polarity (positive wire) than in the direct polarity (negative wire) as showed in figure 7.

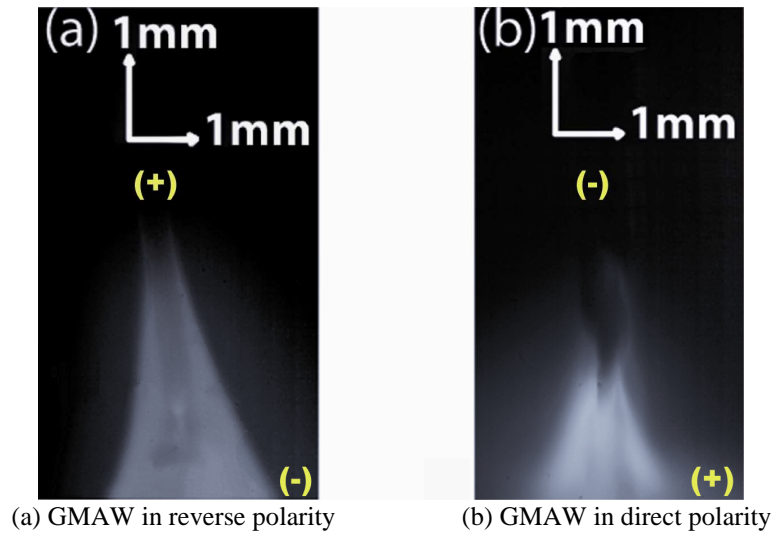


**Figure 7.** Arc attachment to the melting welding electrode,  $I = 330$  A, in Argon

In Zielinska *et al.* [32] work, a high-speed camera (157 images/sec) has been used to investigate the metal transfer and the arc plasma shape in GMAW process. It has been found that the arc plasma in GMAW process is composed of two zones. A bright zone in the center has form of a cone which is surrounded by a peripheral zone of much smaller brightness. Photography of the gas metal arc welding process [32] shows that the anode spot varies markedly with different welding currents. At low welding currents, the anode spot is attached to the bottom of the pendant drop on the end of the electrode. At high welding currents, the anode spot is more diffuse and grows noticeably in size. At sufficiently high currents (for example, above 280 A with 1.2 mm diameter steel electrode) the anode spot fills the drop and begins to climb the cylindrical side walls of the electrodes. Since most of the heat carried to the anode is carried by the welding current, the current in the anode spot causes the cylindrical side walls of the electrode to melt. The end of the electrode forms a tapered geometry. But detailed about the tapered electrode are not clearly distinct. In this second part, we extend the earlier treatment of Zielinska *et al.* [32] by improving the optical layout and by using a faster camera (3000 images/sec). Geometric properties of the melting welding electrode for GMAW process, electrode positive operating in spray mode, are thoroughly determined so that the current density in the anode is experimentally quantified. Thereafter, this experimental current density is used as a boundary condition at the anode surface in conjunction with the theoretical arc model described in the first part of this paper.

### 5. 1 Experiment procedure

The most important welding parameter in GMAW process influencing the droplet formation and the molten electrode is current intensity at its surface. The current density drives the dynamic evolution of the drop and also depends on the instantaneous shape of the drop. The shape profiles of drops detaching from a GMAW electrode can be measured from images of the electrode. However measuring the surface-current emission density along these profiles requires special treatment since a more precise description of where the current emerges from the electrode and how the current density is distributed over the drop is lacking. Even though significant brightness about the drop is observed under certain conditions, this brightness is more an indicator of the arc temperature and composition

than it is of the envelope of current flow. The arc plasma was observed through a narrow band interference filter which transmits at 469.2 nm wavelength (3 nm spectral bandwidth). The system setup and the equipment specifications are detailed by Zielinska *et al.* [32].

The filter cited above is of key importance since it eliminates spectral lines which depend on both the temperature and the electronic density thereby only the continuum of the plasma arc can be seen through. Since the continuum depends mainly on the square of the electronic density and hence on current density, the current-carrying region near the anode cannot be extended substantially beyond the arc boundary suggested by the envelope of brightness. In addition, a diode laser is used to observe the metal-transfer process. The melting wire is illuminated with a H-C3830/40-F4 diode laser and the camera is fitted with an interferential filter centred on the laser wavelength. Then most of the light emitted by the plasma is cut and only the laser light reflected by the melting wire is recorded. The laser source, which is not focused, has a power of 30 W and a wavelength of 838 nm. Successive images were assembled in figure 8 to illustrate the detachment of drops from the electrode. The electrode geometric parameters were measured from the images analysis and averaged.

The images recorded in this experiment are of bead-on-plate gas metal arc welding operated in constant current mode (330 A), that is, the welding current was controlled independently and the welding voltage was regulated about a set point by varying the wire feed speed. In all of the experiments, the electrode was 1.2 mm diameter solid wire (AWS A5.17) shielded with argon, fed at  $9 \text{ m.mn}^{-1}$  through a 21.8 mm diameter gas nozzle. A copper contact tube was mounted flush with the bottom of the gas nozzle and the gas nozzle was always 20 mm above the base plate. The base plate is not visible in all of the images and, using the electrode diameter as a reference, the geometric characteristics of both the arc and the melting electrode can be measured directly from the images. The images were recorded with a high-speed video system at 3000 images per second using the optical technique described in [32], thus the time between images was 333  $\mu\text{s}$ .

## 5.2 Results and discussion

The collection of well-specified, clear images presented here illustrates the condition of a steel GMAW electrode shielded with argon gas operating at constant current of 330 A. The images obtained when the arc plasma is illuminated by the laser light are presented in Figure 8. In the other hand, the area of where the current emerges is clearly observed in figure 9.

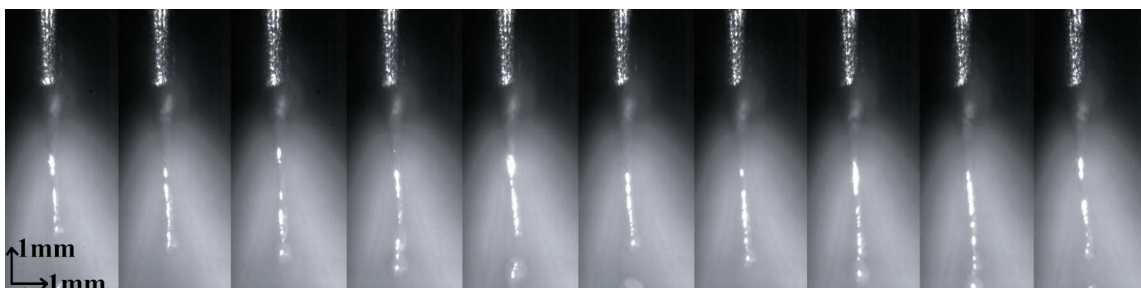


**Figure 8.** The tapering of the welding wire electrode at high welding current, in GMAW process. (Constant current  $I = 330 \text{ A}$  and  $V = 32 \text{ V}$ , reverse polarity; Electrode diameter: 1.2 mm; shielded gas: Argon. Image interval = 333  $\mu\text{s}$ . Filter: 838.0 nm).

From the successive pictures shown in figures 8 and 9, we can see that in GMAW shielded with argon gas, and at high current, the arc is stable, the arc length can be considered invariable, and furthermore, small droplets formed from a tapered electrode. Such a tapered electrode tip geometry, which is shown schematically on Figure 10, does not develop at low welding currents. The tapered tip creates a smaller diameter for attachment of the droplet to the electrode by surface tension forces. This would produce smaller droplets than would be present in the absence of taper formation. There are a

number of consequences of this taper formation. Kim [34] has shown that the melting rate of the electrode is controlled by heat transfer across the liquid-solid boundary between the drop and the solid electrode. Since the taper reduces the area of this boundary, taper formation reduces the rate of melting of the electrode.

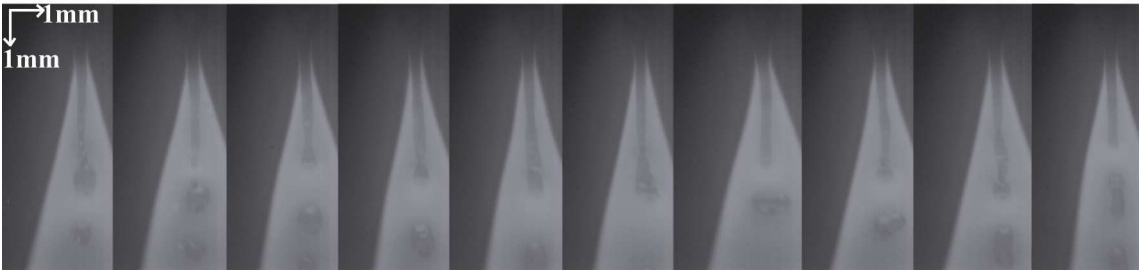


**Figure 9.** Successive pictures of plasma arc in GMAW process.  
 (Constant current  $I = 330$  A and  $V = 32$  V, reverse polarity; Electrode diameter: 1.2 mm; shielded gas: Argon. Image interval = 333  $\mu$ s. Filter: 469.2 nm).

Thus the discrepancy of the calculated temperatures from the MHD model in GMAW process as compared with the experimental data [33] may be explained by examining the validity of the assumptions made in the calculation of the calculated temperatures from the MHD model. One of the most important assumptions is that the electrode should remain cylindrical and maintain its full diameter at the point where the drop is formed. If the geometrical dimensions of the electrode are changed either by surface melting or by deformation, the calculated temperatures will be affected [33]. In figures 8, 9 and 10, we can see that the geometry of the drop holding neck is significantly changed due to formation of a taper at the electrode tip. The tapering of the electrode occurs because the anode spot reaches this surface of the electrode and generates condensation heating on the cylindrical surface of the electrode.

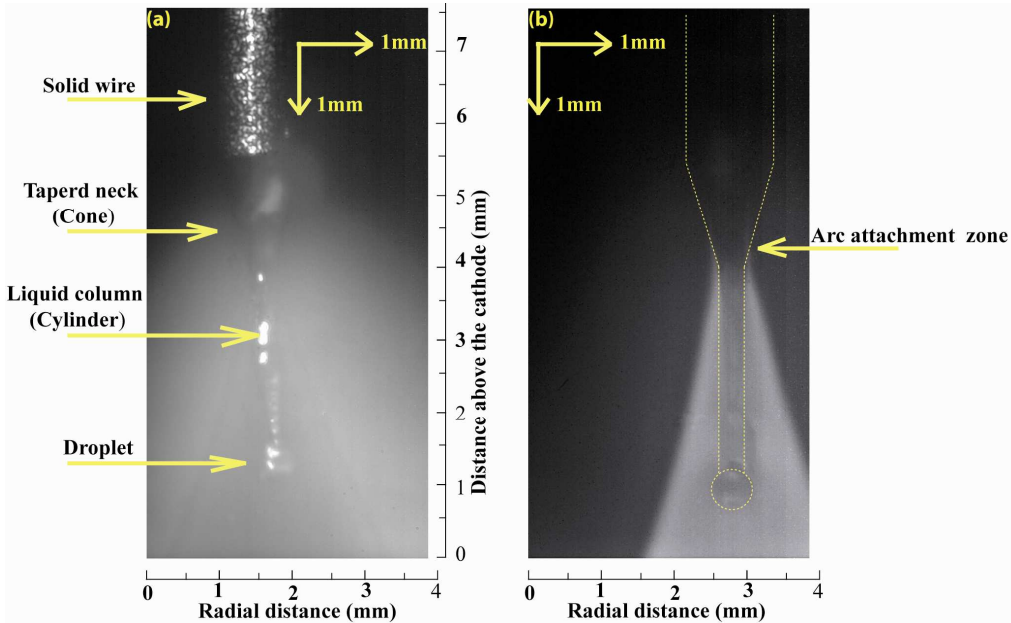


**Figure 10.** Droplet formation at the tapered electrode and arc-anode attachment.  
 (Constant current  $I = 330$  A and  $V = 32$  V, reverse polarity; Electrode diameter: 1.2 mm; shielded gas: Argon. a/ Filter: 838.0 nm, b/ Filter: 469.2 nm).

When enough heat is generated on the surface, the surface will melt and the liquid metal will be swept downward by either the gravitational force and/or the plasma drag force. When this melting and sweeping action occurs over a significant length of cylinder, a taper will develop at the end of the electrode, as it is shown in figure 10. Thus, the assumption of cylindrical electrode which maintains its full diameter at the point where the drop is formed is not justified.

The experimental electrode welding model that we propose in GMAW process consists of two parts: solid and liquid, as shown in figure 11. The solid part is the welding wire of 1.2 mm diameter. The liquid part, which is the tapered electrode, consists of three zones as it is shown in figures 10 and 11. The neck of the taper, which has conical form, is of 1.41 mm length, and the small diameter of the cone is about 0.36 mm. The liquid column has cylindrical form of 0.36 mm diameter and 2.54 mm length. At the end of this liquid column, the droplet with a spherical shape of 0.56 mm diameter is formed. Details of area calculation of these three zones are presented in table 2. As it can be seen in figures 8, 9 and 10, the arc doesn't attach totally the neck of the tapered electrode. Only one sixth of the surface of the tapered neck zone  $S_1$  is considered to be attached by the arc, let this surface be  $\Sigma_1$ ,  $\Sigma_1 = 1/6 S_1$  as shown in table 2. In addition, the droplet has rather a truncated spherical surface  $\Sigma_3$  than a spherical surface  $S_3$ . Thus, the total area from which the welding current emerges is:  $S_{Tot} = \Sigma_1 + S_2 + \Sigma_3$ .

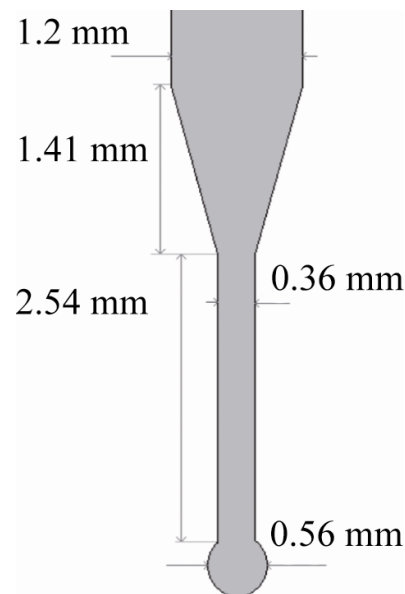


**Figure 11.** A schematic description of the proposed melting welding electrode model used as an anode (reverse polarity) in GMAW process.

(Constant current  $I = 330$  A and  $V = 32$  V, reverse polarity; Electrode diameter: 1.2 mm; shielded gas: Argon).

**Table 2.** Area of the three zones of the melting electrode

Area	$\Sigma_1$ : the taper neck (Cone)	$S_2$ : the liquid column (Cylinder)	$\Sigma_3$ : droplet (Truncated sphere)
Area of the melting anode zone covered by the arc plasma ( $\text{mm}^2$ )	$2.38 \pm 0.01$	$2.87 \pm 0.01$	$0.93 \pm 0.01$
Total area ( $\text{mm}^2$ )	$6.18 \pm 0.01$		

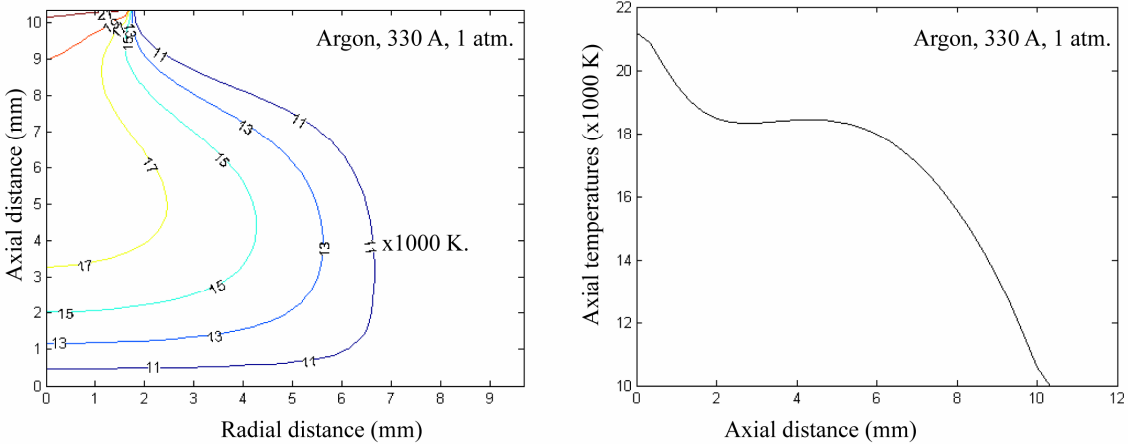
Finally, the welding electrode steel of 1.2 mm diameter, in GMAW process shielded with argon gas,

flowed by a 330 A welding current, has an arc-anode attachment area of 6.18 mm<sup>2</sup> and hence the current density is of 5×10<sup>7</sup> A.m<sup>-2</sup>.

Following the experimental model of the melting-anode presented above, the current density is determined rather than be specified as an arbitrary condition as commonly assumed in literature. In the following section, the MHD model in conjunction with the experimental current density is used to predict temperature distribution in GMAW arc.

5. 3 Arc column calculations

In GMAW, both the cathode and the anode are melted by the arc. Hence, the cathode is non-thermionic and the cathode region is under high pressure due to the impinging plasma jet. The physics of the cathode-fall region and the thermal balance at a non-thermionic cathode are not well understood. Therefore, we have chosen to use a similar treatment of the energy source term at the cathode boundary as used in GTAW [38]. For GMAW, emission of electrons from the cathode might be due to thermo-field emission and there may be important space charge effects in front of the cathode surface [19, 24]. Thereby, except for the current density that flows through the anode surface, the cathode potential and the anode temperature, all the other boundary conditions are the same one that those described in section 2.2. Thus, we set a uniform current density  $J_0$  of 5×10<sup>7</sup> A.m<sup>-2</sup> on the anode surface, defined by the input current divided by the area of cross section of the anode, as mentioned above, whereas the potential is set to zero at the workpiece used as the cathode. The value of the anode temperature determined experimentally in GMAW is lacking, while the calculated values show a high disparity (see for example [24], [36] and [43]); but anyway it is not really necessary for the calculation. Nevertheless it is required to have an estimation of the plasma temperature just under the wire: in a first time, we have taken the value of about 21000 K obtained by Haidar in similar conditions [24], which may seem high considering the relatively low current densities. Figure 12a shows a large arc column, which is due to the diffuse attachment mode. It is seen that the trends of the isotherms are in fair agreement with spectroscopic measurement [33], but the maximum temperature differs noticeably. This is due to the fact that the metal vapors are omitted in this study. Gleizes *et al.* [39] showed that metal-vapor contamination to the arc leads to an increase in the energy loss by the radiation, especially at lower temperatures. Zielinska *et al.* [33] and Valensi *et al.* [42] have shown that not only the maximum temperature is less than 15000 K but this maximum temperature is located away from the arc axe as well, which suggest the presence of metal vapors in the plasma particularly near the cathode and the anode regions.



a-  $T = 21000$  K under the wire, taken from the literature [24]

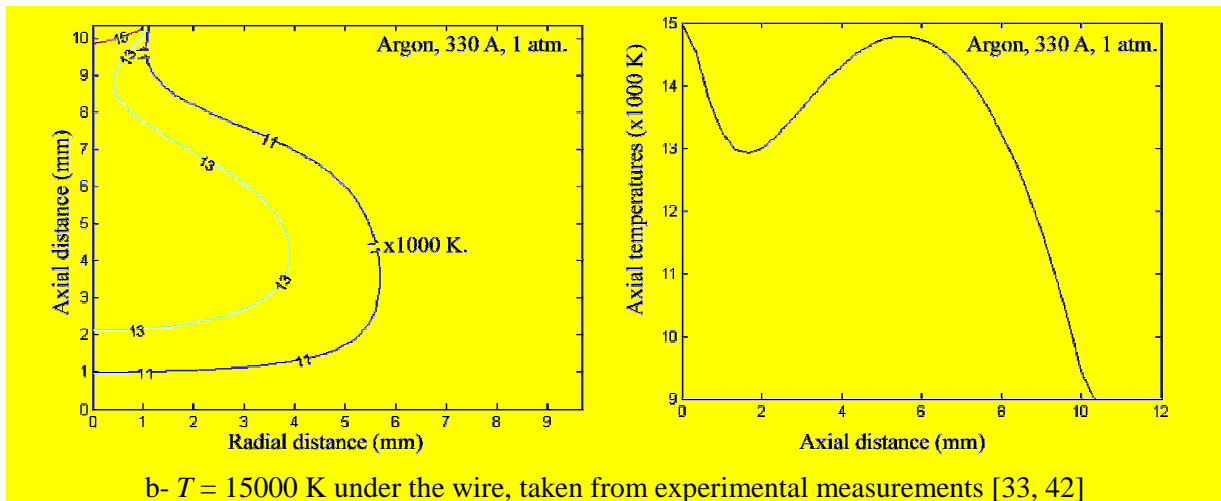


**Figure 12.** Predicted isotherms of a 330 A arc, 10 mm long in argon (GMAW process in reverse polarity -  $P = 1$  atm -  $J_0 = 5 \times 10^7$  A.m<sup>-2</sup> on the anode surface).

Predicted isotherms of a 330 A arc, 10 mm long in argon for this value are shown in Figure 12b. It can be seen that for lower temperatures the arc spreads out less than for higher temperatures like in figure 12a which is in agreement with arcs obtained by relatively low current densities. It should be noted that changing the current density results in a low temperature on the axis of the arc column, which seems to have been observed in the some experimental works that exist in the literature [32, 42]. Nevertheless, it is difficult to exactly compare with these experimental data, because they are difficult to perform on the axis due to the passage of liquid metal droplets, and the authors generally dismiss the central zone of the plasma.

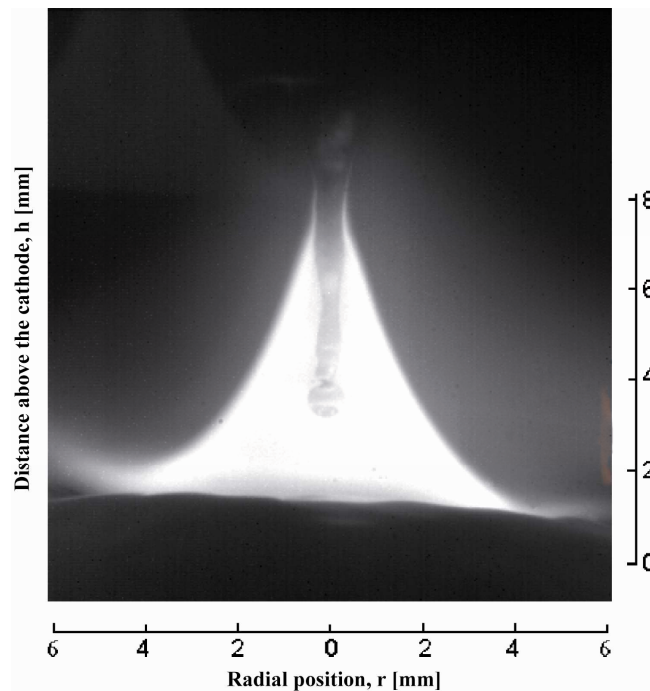


**Figure 13.** GMAW arc. Arc-attachment (Constant current  $I = 330$  A and  $V = 32$  V, reverse polarity; Electrode diameter: 1.2 mm; shielded gas: Argon. Filter: 469.2 nm).

In the other hand, Dunn et al. [40] showed that even small amounts of iron vapors increase the electrical conductivity at low temperatures of both helium and argon gases, which can significantly affect the arc configuration and current density distribution and, consequently, the energy input to the workpiece. Razafinimanana et al. [41] reported that an increase in electrical conductivity, resulting from the presence of metal vapors, leads to an expansion of the conduction channel of an electric current. Figure 13 shows arc configuration for GMAW process, electrode positive, operating in spray mode. It can be seen that even if the cathode is a non-thermionic electrode, the arc spreads over a large surface of the cathode, which could be explained by the presence of metal vapors as introduced above. However, here, our purpose is to determine the trends of the isotherms versus the current density assumed at the anode. The arc-anode attachment region spreads over a large area of the melting anode, resulting in a current density of  $5 \times 10^7 \text{ A.m}^{-2}$ , which is ten times smaller than those proposed by Haidar et al [24] and Hu et al [35-36]. In their work, they considered that the totality of the current flows through the narrow neck of the droplet, consequently, a high welding current that flows through a small surface, results in an overestimated current density and hence a narrow arc column.

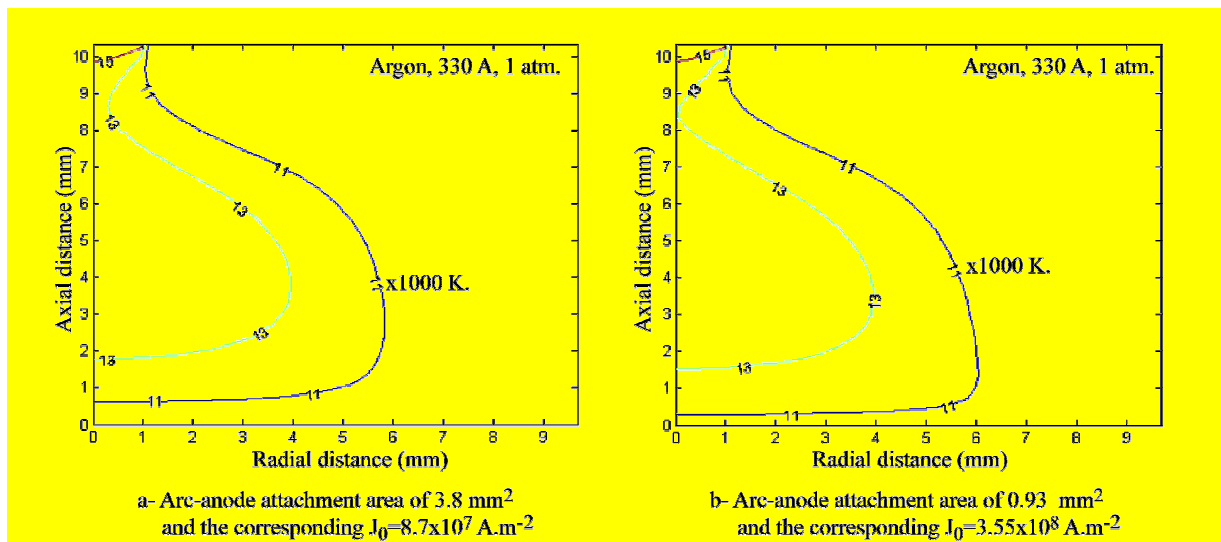


**Figure 14.** Predicted isotherms of a 330 A arc, 10 mm long in argon (GMAW process in reverse polarity -  $P = 1 \text{ atm}$  -  $T = 15000 \text{ K}$  under the wire [33, 42]).

In figure 14, we show results for calculations performed using smaller arc-anode attachment for a temperature fixed to  $15000 \text{ K}$  under the wire [33, 42]. For the arc attachment to the anode limited to an area of  $S_2 + \Sigma_3 = 2.87 + 0.93 = 3.8 \text{ mm}^2$ , which represents 61% of the total area of the effective surface attachment ( $6.18 \text{ mm}^2$ ), the corresponding current density would be about  $8.7 \times 10^7 \text{ A.m}^{-2}$ , which represents an increase in current density of 74% compared with the case of full attachment. If the arc attach only on the droplet ( $\Sigma_3 = 0.93 \text{ mm}^2$ ), which represents 15% of the total area of the effective surface attachment, the current density would be about  $3.55 \times 10^8 \text{ A.m}^{-2}$ , which is ten times higher than our new current density. Figure 14, shows isotherms corresponding to these surface attachments. It can be seen clearly that little surface attachment results in a narrow arc.

We showed in the section above that the current emerges from a large area of the melting anode, thus, it is worth mentioning that current density in GMAW higher than  $10^7 \text{ A.m}^{-2}$  seems to be not justified for welding current less than 330 A.

For further improvement of quality control in GMAW process, plasma temperature has to be estimated rather in situ. This could be done by using the proposed welding electrode model in conjunction with the automatic determination of the geometrical electrode parameters. The counter

detection, shown in the right hand side of figure 15, seems to be a powerful method for the instantaneous determination of such geometrical shapes.

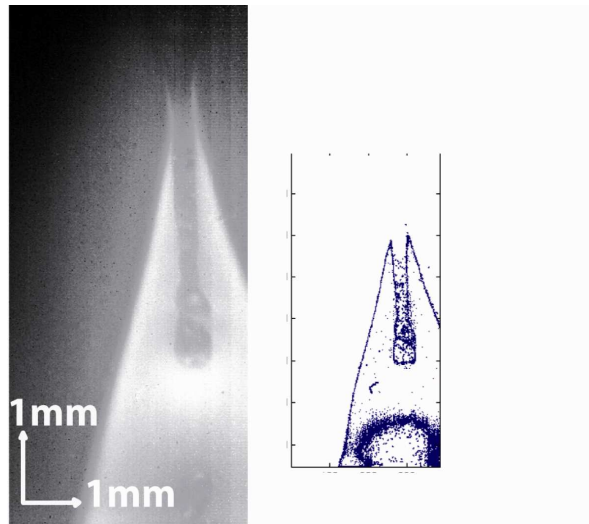


**Figure 15.** Automatic determination of the geometric electrode properties in GMAW process (reverse polarity), by using contour detection technique.

## 6. Conclusion

A numerical model of a free-burning arc in atmospheric-pressure argon plasma has been developed to analyze a stationary Gas Tungsten Arc welding (GTAW) process. Solutions of the conservation equations with appropriate boundary conditions have been obtained for atmospheric pressure argon arcs in a current range from 100 A to 300 A and electrode gap of 10 mm. Both the temperatures and the current density are extremely sensitive to the current density boundary condition close to the cathode. The predicted arc temperature and current density distributions are in good agreement with the measurements in the literature. The discrepancies, near the cathode and anode regions may be due to arc-electrode interactions.

The model developed has been extended to Gas Metal Arc Welding (GMAW) process. In GMAW process, the electrodes have to be included as dynamic entities, so it will be interesting to introduce realistic boundary conditions for the current density in the anode. We showed in the second section of this work that the current density boundary can easily be obtained if the shape of the welding electrode used as an anode is known. High-speed camera (3000 images/sec) was used to get geometrical dimensions of this melting anode, and by using specific narrow interference filters (469.2 nm, 838.0 nm) we managed to observe the metal-transfer process and how the current density is distributed over the drop. Thus, the total area of where the current emerges was thoroughly determined in the case of mild steel consumable electrode (AWS A5.17) of 1.2 mm diameter shielded by argon gas, and flowed by a 330 A current. It is worth mentioning that current density in GMAW higher than  $10^7$  A.m<sup>-2</sup> seems to be not justified for welding current less than 330 A. It's hoped that melting electrode model presented here will provide guidance of authors attempting to develop more complete models of the GMAW melting process.

## 7. References

- [1] Patankar S V, "Numerical Heat Transfer and Fluid Flow" (McGraw-Hill, New York, 1980).
- [2] Hsu K C, Etemadi K and Pfender E 1983 *J.Appl.Phys: Appl.Phys.* **54** 1293–301.
- [3] Kovitya P and Lowke J J 1985 *J.Phys.D: Appl.Phys.* **18** 53–70.
- [4] Ushio M, Szekely J and Chang C W 1981 *Ironmaking Steelmaking* **6** 279–86.
- [5] Kovitya P and Cram L E 1986 *Welding Journal* **65** 34–38.

- [6] Wu C S, Ushio M and Tanaka M 1997 *Comput.Mater.Sci.* **7** 308–14.
- [7] Goodarzi M, Choo R and Toguri J M 1997 *J.Phys.D: Appl.Phys.* **30** 2744–56.
- [8] Zacharia T, David S A, Vitek J M and DebRoy T 1990 *Metall.Trans. B* **21B** 600–3.
- [9] David S A, DebRoy T and Vitek J M 1994 *MRS Bull.* **19** 29–35.
- [10] Zacharia T, David S A, Vitek J M and Kraus H G 1995 *Weld.J.***74** 353s–62s.
- [11] Lei Y, Shi Y, Murakawa H and Ueda Y 1997 *Trans.JWRI Osaka Univ.* **26** 1–8.
- [12] Kim W H, Fan H G and Na S J 1997 *Numerical Heat Transfer A* **32** 633-52.
- [13] Fan H G, Tsai H L and Na S J 2001 *Int.J.Heat Mass Transfer* **44** 417–28.
- [14] Winkler C, Amberg G, Inoue H, Koseki T and Fuji M 2000 *Sci.Technol.Weld.Joining* **5** 8–20.
- [15] Choo R T C and Szekely J 1992 *Weld.J.* **71** 77–93s.
- [16] Goodarzi M, Choo R, Takasu T and Toguri J M 1998 *J.Phys.D: Appl.Phys.* **31** 569.
- [17] Zhu P, Lowke J, Morrow M 1992 *J.Phys.D: Appl.Phys.* **25** 1221–2130.
- [18] Tanaka M, Terasaki H, Ushio M and Lowke J J 2002 *Metall.Mater.Trans. A***33** 2043–52.
- [19] Haidar J 1998 *J.App.Phys.* **87-7** 3518-3528.
- [20] Block-Bolten A and Eagar T W 1984 *Metall.Trans.* **15B** 461.
- [21] Cieslak M J and Fuerschbach P W 1988 *Metall.Trans.* **19B** 319.
- [22] Hsu K C and Pfender E 1983 *J.App.Phys.* **54** (3) 1293–1301.
- [23] Haidar J and Farmer A J D 1993 *J.App.Phys.* **26** 1224-1229.
- [24] Haidar J 1998 *J.App.Phys.* **31** 1233-1244.
- [25] Lowke J J, Kovitya P and Schmidt H P 1992 *J.Phys.D: Appl.Phys.* **25** 1600-1606.
- [26] Tanaka M, Lowke J J, 2007 *J.Phys.D: Appl.Phys.* **40** R1–R23.
- [27] Lowke J J, Morrow R, Zhu P, Haidar J, Farmer A J D and Haddad G N 1992 *Journal of high temperature chemical processes*, Coll-Suppl au n°3-1 499-555.
- [28] Sansonnens L, Haidar J and Lowke J J 2000 *J.App.Phys.* **33** 148-157.
- [29] Lowke J J, Morrow R and Haidar J, 1997 *J.App.Phys.* **30** 2033–2042.
- [30] Fan H G, Na S-J and Shi Y W 1997 *J.App.Phys.* **30** 94-102.
- [31] Hu J and Tsai H L 2006 *J.App.Phys* **100** 2644-2649.
- [32] Zielinska S, Pellerin S, Valensi F, Dzierzega K, Musiol K, de Izarra C and Briand F 2008 *European Physical Journal - Applied Physics* **43-1** 111-122.
- [33] Zielinska S, Pellerin S, Valensi F, Dzierzega K, Musiol K, de Izarra C and Briand F 2007 *Plasma Sources Science and Technology* **16** 832-838.
- [34] Kim Y S 1989, “Metal transfer in gas metal arc welding”, Ph.D thesis, M.I.T., Cambridge, Mass.
- [35] Hu J and Tsai H L 2007 *International journal of Heat and Mass Transfer* **50** 833-846.
- [36] Hu J and Tsai H L 2007 *International journal of Heat and Mass Transfer* **50** 808-820.
- [37] Hsu K C and Pfender E 1983 *J.App.Phys.* **54** (7) 3818–3824.
- [38] Jonson P G, Eagar T W Szekely J 1995 *Metall.Trans. B* **26B** 383-395.
- [39] Gleizes A, Gonzalez J J, Liani B, and Raynal G 1993 *J. Phys. D: Appl. Phys.* **26** 1921-27.
- [40] Dunn G J Eagar T W 1986 *Metall. Trans. A* **17A** 1865-71.
- [41] Razafinimanana M, Hamidi L E, Gleizes A, and Vacquier S 1995 *Plasma Sources Sci. Technol.***4** 501-10.
- [42] Valensi F, Pellerin S, Boutaghane A, Dzierzega K, Zielinska S, Pellerin N and Briand F 2010 *J.Phys.D: Appl.Phys.* **43** 434002.
- [43] Wang Y and Tsai H L 2001 *Int.J.Heat Mass Transfer* **44-11** 2067–80.